Polymer Testing 102 (2021) 107323

Contents lists available at ScienceDirect

Polymer Testing

journal homepage: www.elsevier.com/locate/polytest

# Low temperature fatigue crack propagation in toughened epoxy resins aimed for filament winding of type V composite pressure vessels

Fabian Hübner [a], Alexander Brückner [a], Tobias Dickhut [b,1], Volker Altstädt [a], Agustín Rios de Anda [c,*], Holger Ruckdäschel [a,**]

[a] Department of Polymer Engineering, University of Bayreuth, Universitätsstrasse 30, 95447, Bayreuth, Germany
[b] MT Aerospace AG, Franz-Josef-Strauß-Straße 25, 86153, Augsburg, Germany
[c] Institut de Chimie et des Matériaux Paris-Est, Université Paris-Est Créteil, UMR 7182 CNRS, 94320, Thiais, France

ARTICLE INFO

*Keywords:*
Epoxy
Mechanical testing
Fatigue crack propagation
Low temperature
Toughener
Low viscosity

ABSTRACT

In this study, application relevant toughened epoxy-amine formulations were investigated regarding their mechanical behavior at low temperatures and compared to a non-toughened reference. The application-oriented resins are based on reactive diluent-modified diglycidylether of bisphenol A (DGEBA) which were tested at 22 °C and −50 °C in regard to their fracture toughness ($K_{IC}$) and fatigue crack propagation ($da/dN$) behavior. The $E'$ and $E''$ moduli and the corresponding glass transition temperatures $T_g$ were determined via dynamic mechanical thermal analyses (DMTA) which also described the influence of the block copolymeric toughener on the epoxy resin network. The plastic zone size, calculated during crack propagation, reveals the temperature dependent toughener-matrix interaction. The prevailing energy dissipation mechanisms were correlated with the changes of $E'$. SEM micrographs confirm the superior performance of the toughened system at −50 °C by the decrease of the fatigue cack propagation slopes and highlight the trends of the materials low temperature behavior.

## 1. Introduction

Epoxy resin systems are widely used as engineering polymers for adhesives, coatings, housings. Due to their low viscous appearance in uncured state, these systems are also ideal for manufacturing lightweight composite materials [1]. Due to their excellent resistance to environmental and chemical media, as well as their good creep behavior, they offer a perfect balance in processability and mechanical performance for reinforced aerospace propulsion storage modules [2–4.]. Indeed, in order to being able to increase a rockets payload, lightweight aerospace fuel vessels are currently under development. The specific processing route depends on the vessel geometry and size, thus the functional properties of epoxy resins as potential matrices, namely the glass transition temperature ($T_g$), the tensile strength, and the fracture toughness have to be evaluated. While large scale rotational symmetric parts are manufactured by automated tape laying (ATL) with prepregs, smaller pressure vessels in the range of 10–50 L for automotive applications are manufactured via filament winding. [5] Balancing the right gel-time, reactivity, and viscosity of the matrices is already challenging. Additionally, suitable toughness modification to ensure an optimum performance in low temperatures environments of gaseous hydrogen (−50 °C) is a current research topic. Increasing the resistance against cracking especially at lower temperatures can be carried out by adding high molecular weight curing agents to flexibilize the network and decrease the crosslink density. [6–8]

Another, more classical solution, to increase the crack propagation resistance is considering common toughening agents such as organic rubber particles or spherical silica particles [9–17]. Even though they successfully improve the materials toughening behavior, they exhibit various disadvantages such as particle filtration, a drop of Young's modulus by rubber particles and increasing viscosities. The latter is a major drawback as regards LCM and wet winding process. Thus, to overcome these issues, a series of new generation additives such as preassembled or reaction induced assembling Core-Shell-Particles (CSP)

* Corresponding author.
** Corresponding author.
*E-mail addresses:* rios@icmpe.cnrs.fr (A. Rios de Anda), ruckdaeschel@uni-bayreuth.de (H. Ruckdäschel).
[1] Current address: Institute Aeronautial Engineering, Universität der Bundeswehr München, Werner-Heisenberg-Weg 39, 85,579 Neubiberg

https://doi.org/10.1016/j.polymertesting.2021.107323
Received 7 May 2021; Received in revised form 11 June 2021; Accepted 27 August 2021
Available online 4 September 2021

have been introduced in the past years. SBS- PBu-SBS core--shell-particles with an energy dissipating rubber core or PCL-PDMS- PCL with a low temperature active silicone core, [18–24] and Block Co-Polymer (BCP) based CSP-like additives, which phase separate in the epoxy matrix by reaction induced phase separation (RIPS) or self-assembly (SA) [25–31] can be mentioned here. Those latter tougheners boost the critical stress intensity factor $K_{IC}$ (i.e., a direct measurement on the increase of toughening behavior) efficiently with very low volume fractions and show no filtration or viscosity changes due to inherent precipitation while curing. The toughening mechanisms at room temperature are very well known in literature. However low temperature properties, especially in fatigue crack propagation, essentially required for the construction of long-term cycled thermosetting composite components such as filament winded hydrogen vessels are not highlighted in greater depth in combination with applicative relevant epoxy resin systems with focus on industrial processing. Indeed, a special requirement for pressure vessels is low temperature performance for fuel liquids, e.g., liquid hydrogen, where the storage tank undergoes temperatures down to 20 K. Thus, materials with an enhanced resistance to microcracking at cryogenic temperatures has started to be studied in thermoset-polymers and fiber reinforcement applications. [2,32–35]

Microcracking might result from a thermal expansion mismatch between the matrix and the fibers. This can be avoided or reduced by modifying the matrix to a certain fracture toughness level [32,36–42] In the past several years, the investigation of dynamic fatigue crack propagation (i.e. *da/dN* tests) phenomena, pioneered by Paris and Erdogan [43,44] has gained great interest in the case of functional thermoset materials. Indeed, this property is of paramount concern for stress and temperature cycled composite parts in aerospace and the automotive industries, with pressure vessels being an application, as such experiments can predict the cycle lifetime of a part that has suffered a crack over its applicative lifetime. In that regard, *da/dN* measurements are able to characterize the variation in fatigue crack propagation behavior in presence of additives or charges. Various types of additives have demonstrated to improve this materials property, for instance silicone or CTBN [45], inorganic nanosilica [46] of various sizes and shapes [47, 48] and finally, BCP tougheners [49]. Nevertheless, most of the *da/dN* tests are carried out at room temperature, but information about the materials behavior during low temperature service conditions are missing. As such this works aims to study the fatigue crack propagation behavior of BCP-toughened epoxy resins for filament winding at −50 °C and at room temperature. These characterizations are linked to the material's inherent properties such as the glass transition temperature $T_g$, their Young's modulus, their static fracture toughness and the BCP particle distribution in regard to fatigue crack propagation behavior. This approach allows to describe the physico-chemical phenomena leading to a variation on the materials behavior at specific temperatures. By considering such an approach, the behavior of the investigated materials can be understood for future composite pressure vessel applications.

## 2. Materials

*LITESTONE*™ epoxy systems developed for LCM were kindly supplied by *Olin Corporation* (*Blue Cube Assets GmbH & Co. KG,* Stade, Germany). Both, the toughened and non-toughened systems are based on modified epoxy resin *LITESTONE*™ *2100E* with an epoxy equivalent weight (EEW) of 170 g/mol and consist of >75 wt% of DGEBA and <25 wt% glycidylether based reactive diluent [50]. Thus, low viscosities of below 3000–3500 mPa*s achieve advanced wetting properties and reduced infusion times. Two aliphatic diamine curing agent mixtures based on, poly-oxy-propylene-diamine and a mix of cycloaliphatic diamines, one with (*LITESTONE*™ 2117H) [51] and one without (*LITESTONE*™ 2107H) toughening agent [52] were used in this study. The toughening agent based on a phase separating amphiphilic block copolymer [53] tends to form 350–400 nm sized micellic structures while curing, resulting in milky resin castings. The 2K formulation was used as received from the supplier.

## 3. Experimental

### 3.1. Curing and sample preparation

The two investigated epoxy resin systems were mixed at a weight ratio of 100:28 (*2100E + 2107H*) and 100:29 (*2100E + 2117H*) for 20 min using an *IKA* lab stirrer at 300 rpm. Afterwards, the liquid mixture was degassed for 10 min below 10 mbar prior to curing until no air entrapments were identified. The epoxy-amine mixture was poured into vertical aluminum molds of dimensions 200 × 200 × 4 $mm^3$. The curing for both systems took place in a *Memmert* convection oven with a curing process of 30 min 70 °C for gelation and 4 h at 110 °C for post-curing according to the suppliers datasheet. Afterwards the material was cooled down for 6 h to room temperature to prevent internal stress. Samples with corresponding geometries according to the ISO standards for each experiment were either cut with a *Mutronic DIADISC5200* diamond plate saw, or CNC milled by a *Mutronic Diadrive 2000*.

### 3.2. Dynamic mechanical thermal analysis

Dynamic mechanical thermal analysis (DMTA) was used to measure of the materials complex – storage (E′) and loss moduli (E'') versus the change of temperature. The glass transition temperature $T_g$ was determined by the maximum of the loss factor *tan δ*. A *Gabo Eplexor 500 N* (*Gabo Qualimeter Testanlagen GmbH* Ahlden, Germany) was used in single cantilever mode. The samples with a geometry of 50 × 10 × 2 $mm^3$ were tested at a heating rate of 3 K/min from −100 to 120 °C, a frequency of 1 Hz in unidirectional tension loading, and a deformation of 0.1% in the linear regime. The same procedure was carried out with a Rheometric scientific RDAIII from 20 to 180 °C, but to measure storage modulus $G'$ in torsion to precisely determine the network density $\nu_C$. Storage modulus $G'$ in the rubbery state was taken to calculate this bulk material value according to equation (1) [54,55]:

$$V_C = \frac{G'}{R^*T} \quad (1)$$

Here, $R$ is the gas constant (= 8.314 J/mol K) and $T$ is $T_g$ +50 K in absolute temperature.

### 3.3. Mechanical characterization

#### 3.3.1. Tensile & compression testing

The tensile modulus was measured by tensile testing of 5 specimen with 1B dog-bone specimens in dimensions 150 × 10 × 4 $mm^3$. They were tested with a crosshead speed of 5 mm/min according to DIN EN ISO 527-2. The samples yield behavior, was investigated by compression testing. Five samples per formulation of dimensions 10 × 10 × 4 $mm^3$ were tested with a crosshead speed of 5 mm/min according to EN ISO 604. Both tensile and compression tests were done on a ZwickRoell Z050 universal testing machine (ZwickRoell GmbH & Co. KG, Germany) equipped with a load cell of 20 kN and a temperature chamber for compression cooling.

### 3.4. Fracture toughness

Quasi static mechanical tests were carried out to characterize the critical stress intensity factor $K$ in Mode I ($K_{IC}$) with ISO 13586. Five samples per formulation were tested on a ZWICK Z020 equipped with a load cell of 5 kN and a temperature chamber operating with a compressor cooler allowing testing temperatures down to −50 °C. The room temperature samples references were measured at 22 °C with 50% r.H.

According to ISO 13586 CT-specimens with a geometry of 39.6 ×

41.25 × 4 mm$^3$ and a sharp crack tip were tested with a traverse speed of 10 mm/min. KIC was then calculated according to Equation (2):

$$K_{IC} = \frac{F\,max}{d\ \$\ \sqrt{w}}\$f\ (\frac{a}{w}) \quad (2)$$

where $F_{max}$ is the maximum force leading to crack propagation, $d$ is the specimen thickness, $w$ (i.e. = 33 mm) is the efficient width and $f\,(a/w)$ is a geometrical term coming from the initial sharp crack length a and the sample geometry [46]. From $K_{IC}$ values, the fracture energy $G_{IC}$ was calculated according to Equation 3.

$$G_{IC} = \frac{(K_{IC})^2}{E}\$(1-\upsilon^2) \quad (3)$$

$E$ is the Young's modulus derived from temperature dependent tensile testing and υ is the Poisson's ratio, taken to be 0.35 for epoxy in the glassy state.

The diameter of the plastic zone $d_p$ was calculated according to Irwin's theory along Equation (3), with the assumption of a plane-strain deformation behavior of brittle epoxy [16, 56]

$$d_p = \frac{1}{3\pi}(\frac{K_{IC}}{\sigma_Y})^2 \quad (4)$$

where $\sigma_Y$is the compression yield strength, derived from the compression testing. Compression testing was carried out since epoxy resins as brittle materials do not tend to yield under tensile load, especially under low temperature. The tensile yield behavior was calculated by multiplying the compression yield value by roughly 0.793 according to [16, 56].

The notion of the plastic zone dp is an estimation that allows to compare materials as regards the ease with which a crack propagates. dp can be thought as a locally modified zone of the polymer around the crack in which the local tension in the material provokes a very local plasticization. However this must not be fully compared with the meso- and macroscopic brittle or elasto-plastic behavior of the polymer. Epoxy resins whether at room temperature or low temperature fail in the linear elastic regime and do not tend to yield via a plastic deformation like thermoplastics. In our study, all measurements were done well below $T_g$, thus we would expect our samples to behave as brittle polymers with very localized plasticized zones around the crack tips.

### 3.5. Fatigue crack propagation

The crack growth rate *da/dN* was measured in a time frame of 16 h with a servo hydraulic testing machine *IST Hydro pulse MHF* until unstable crack growth and failure of the specimen took place. Two samples per formulation with the same dimensions as described for fracture toughness measurements were tested since the measurements were very reproducible. A *MTS* clip-on gauge was fixed on the sample allowing to monitor the crack opening displacement $\delta$ at a testing frequency of 10 Hz. The −50 °C testing was carried out in a temperature chamber with an indirect liquid nitrogen evaporation set-up. The temperature was measured directly at the sample in a steady state temperature range of −51 ± 1.5 °C with a sinusoidal temperature oscillation.

The crack growth rate *da/dN* was calculated with the compliance method according to Paris' and Erdogan's empirical crack propagation law [43, 44]

$$\frac{da}{dN} = C\Delta K^m \quad (5)$$

where, da is the infinite change of the crack length in mm per applied loading cycles N, which is in dependency of a material constant $C$. The applied stress intensity value is expressed by $\Delta K = K_{max}$-$K_{min}$ ($\frac{K_{min}}{K_{max}}$set to 0.1) and the slope of the curve is represented by $m$.

The crack tip opening displacement $\delta$for plane-strain conditions which embodies the range of the crack tip during the load cycle, was calculated according to Equation (6).

$$\delta = \frac{\Delta K_{max}{}^2}{E\sigma_y}\$(1-\upsilon^2) \quad (6)$$

Analogous to the plastic deformation around the crack tip derived from static measurements, the dynamic plastic zone was calculated with $\Delta K_{max}$ from *da/dN* measurements according to Equation (7) [57]:

$$d_p = \frac{1}{3\pi}(\frac{\Delta K_{max}}{\sigma_Y})^2 \quad (7)$$

### 3.6. Scanning electron microscopy

The fractured cross section of the CT specimens after testing at room temperature and at −50 °C was characterized by a *Zeiss Gemini 1530* Scanning Electron Microscope. Surfaces were platinum-sputtered with a thickness of approximately 5–10 nm. The SEM acceleration voltage used was 3 kV.

## 4. Results

### 4.1. Dynamic-mechanical thermal analysis (DMTA)

DMTA measurements were undertaken to obtain a first insight on the evolution of the thermomechanical behavior upon the temperature performance for the studied samples.

Fig. 1a shows the complex modulus $E^*$ and the *tan* $\delta$ values of both epoxy-amine systems in a temperature range from −120 °C to +120 °C. It is firstly observed that the toughened epoxy system exhibits a higher complex modulus $E^*$ throughout the whole temperature range in comparison to the non-toughened neat resin. A possible stiffening effect of the particles on the epoxy network can be explained as follows: both studied materials show a change of the slope related to a decrease of the modulus from 6000 MPa at −120 °C down to roughly 2700 MPa at room temperature. This drop is directly related to the beta relaxation of these materials, which corresponds to local aromatic ring motions within the chain segments [58]. It is observed in Fig. 1b that the peak corresponding to the beta relaxation is definitely widened and shouldering

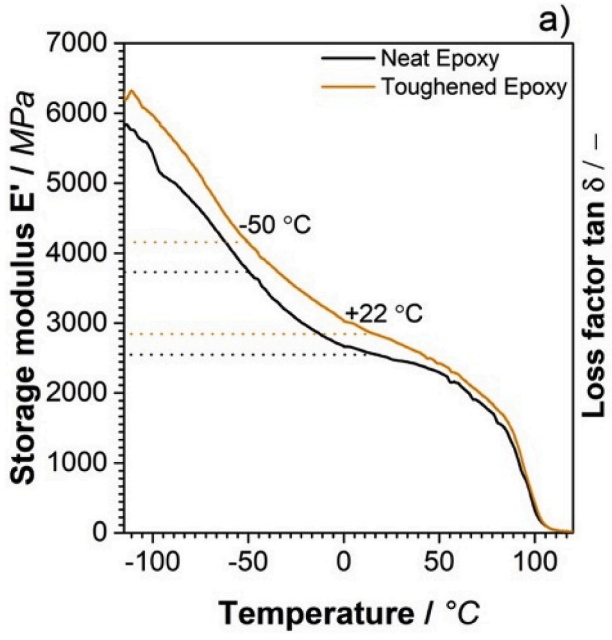


**Fig. 1a.** Complex modulus of neat and toughened epoxy at 1 Hz with 3 K/min heating rate in dependency of temperature.

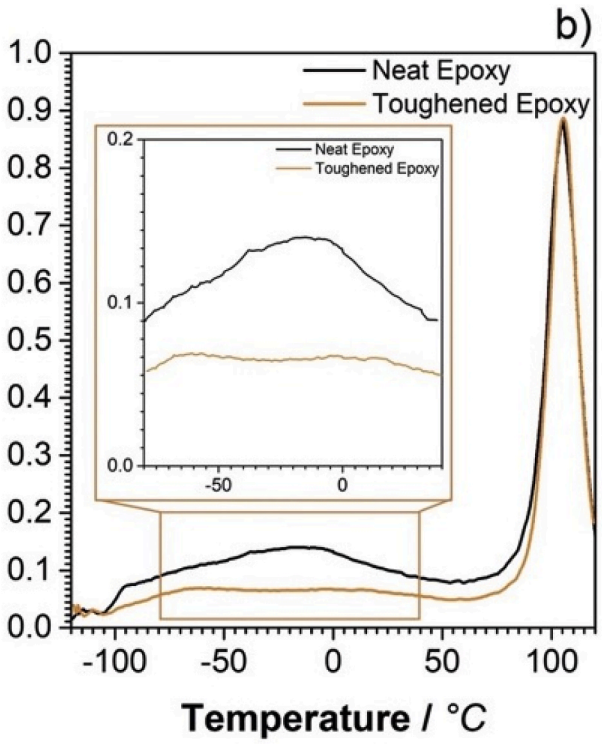


**Fig. 1b.** Loss factor tan δ *of neat and toughened epoxy as a ratio of E′ and E′′*

seems to appear in presence of the BCP-toughener. This indicates that a higher stiffness can be related to a change of the molecular motion in the epoxy's beta relaxation coming from the nano-sized toughener particles (see Fig. 1b).

Additionally, it is also observed that the $T_g$ and the width of the peak corresponding to this transition, listed in Table 1, are not influenced by the presence of the toughener, which is a very positive phenomenon. This means that there is surprisingly no negative effect on the material's molecular mobility at the chain scale. Furthermore, the calculated materials crosslink density increases slightly from 2363 to 2703 mol/m$^3$ by adding the toughener. This means that the particles increase the storage modulus $G'$ taken for the $\nu_C$-calculation in the rubbery regime indirectly. It is widely accepted that the presence of micron-sized or non-compatible particles in epoxy resins leads to a drop on modulus, $T_g$, and crosslink density. Moreover, a previous study conducted by the authors on similar systems containing BCP-CSP, showed a similar trend of increasing functional properties. The increase of the modulus and crosslink density, without modifying the $T_g$, was explained by a positive synergy between the uncured matrix and the particles, which would act as nucleation point, where accelerated curing occurs. This was proved by the use of $^1$H DQ Time domain NMR experiments [59]. The observations in the previous study, lead us to suggest that the presence of the toughener yields two populations of chains with different molecular mobility at the local scale (i.e. at the scale of aromatic rings), leading to two distinct beta relaxations in the material [55,60]. The shouldering in the DMA diagram observed at ca. −20 °C would correspond to the local motions of chains closest to the BPC-CSP particles whereas the shouldering at −80 °C would correspond to the local motions of the bulk matrix [20]. Furthermore, even though an increase on the calculated crosslink density is observed, the $T_g$ does not vary as these systems are highly crosslinked and it might be possible that the critical theoretical crosslink density yielding the maximum theoretical $T_g$ of these matrices has been attained for both samples.

It is thus seen from DMTA measurements that the overall thermo-mechanical behavior of the epoxy resin is modified by the presence of the BCP toughener, both at the molecular (i.e. beta relaxation) and macroscopic (i.e. complex modulus $E^*$) scale. In order to deepen the materials understanding, the static mechanical properties were characterized at various temperatures to assess the fracture mechanical interaction of the BCP particles with the epoxy matrix.

**Table 1**
Detailed data derived from DMTA measurements.

| | Non-Toughened | Toughened |
|---|---|---|
| | 2100E + 2107H | 2100E + 2117H |
| max. tan δ (Tg) | 105 °C | 105 °C |
| Width at half height | 16.3 °C | 15.4 °C |
| Crosslink density νC | 2363 mol/m$^3$ | 2703 mol/m$^3$ |
| E′ at −50 °C | 3702 MPa | 4152 MPa |
| E′ at 22 °C | 2505 MPa | 2785 MPa |

### 4.2. Quasi static mechanical properties

For a first overview, the tensile tests highlighted in Table 2 show an increased Young's modulus at −50 °C. This stiffening effect as a consequence of the low temperature combined with a reduced elongation at break from roughly 7% to below 2% is in accordance with the literature. But the modulus increase is not as drastic as highlighted before in DMA. This effect can be explained by the measurement setup of DMA in between 0.01 and 0.1% deformation and additionally a higher testing speed at the frequency of 1 Hz which seems to have an influence on the modulus especially at low temperatures. Furthermore, also the tensile strength of the toughened EP increased, the neat one decreased due to the sample's quality which was found to be a crucial parameter in low temperature testing. Every sample imbalance results significantly in a catastrophic failure case. It was also seen that compression testing is not as sensitive to sample quality. Here the two systems show the same increased compression strength of 170 MPa and no influence of the toughener on the macroscopic material properties.

Moreover, for toughened epoxy matrices, toughening is the most pertinent property indicating a variation on functional performances. This property is quantitatively analyzed by measuring the critical stress intensity factor $K_{IC}$. Additionally, the fracture energy $G_{IC}$ is also a pertinent parameter as it takes into account the materials Young's modulus.

Firstly, comparing the room temperature measurements, an increase of $K_{IC}$ from 0.69 ± 0.04 to 1.05 ± 0.07 can be observed in Fig. 2. By doubling the fracture energy $G_{IC}$, the expected toughness enhancement by the BCP is demonstrated. Moreover, a rise of $K_{IC}$ within the neat system at −50 °C can be observed. The literature explains this effect by a contracting network, which results in higher forces required for crack propagation which induce instable crack growth. This is even more significant in cryogenic environments such as liquid nitrogen [6,61,62].

**Table 2**
Static mechanical properties derived from tensile and compression testing.

| | Testing Temperature | Neat 2100E + 2107H | Toughened 2100E + 2117H |
|---|---|---|---|
| Young's modulus E [MPa] (Tensile) | +22 °C | 3140 ± 47 | 3050 ± 36 |
| Young's modulus E [MPa] (Tensile) | - 50 °C | 3478 ± 166 | 3454 ± 264 |
| Compression Yield strength [MPa] | +22 °C | 91.4 ± 2.5 | 93.6 ± 1.1 |
| Compression Yield strength [MPa] | - 50 °C | 170.2 ± 5.1 | 170.3 ± 1.7 |
| Tensile strength [MPa] | +22 °C | 74.2 ± 1.8 | 70.4 ± 0.6 |
| Tensile strength [MPa] | - 50 °C | 63.1 ± 2.9 | 74.54 ± 4.1 |
| Elongation at break [MPa] | +22 °C | 6.9 ± 0.2 | 7.63 ± 0.4 |
| Elongation at break [MPa] | - 50 °C | 1.9 ± 0.1 | 2.5 ± 0.16 |

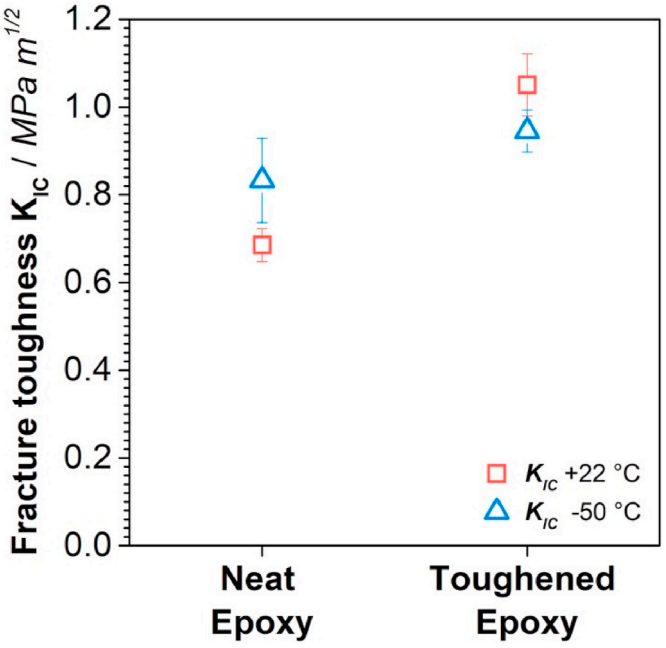


**Fig. 2.** *Fracture toughness measurements of toughened and non-toughened epoxies at 23°C and -50 °C.*

Distinctly is the opposite effect in the toughened epoxy highlighted in Fig. 2. $K_{IC}$ as well as $G_{IC}$ drops towards the level of the neat resin system. This indicates a more brittle behavior. In dependency of the quasi static-testing, fast crack propagation observed with a CT specimen takes place, thus decreased interaction of the BCP toughener at lower temperature at high deformation rates is a consequence. Additionally, the separated effect of an increased matrix ductility occurs at lower temperature, higher than the neat epoxy samples. Hence the macroscopic fracture morphologies are shown in Fig. 3. These images present in a graphic manner the role of the particles in the resin, namely their influence on the fracture toughness and dissipation mechanisms as a function of the testing temperature.

While the non-toughened epoxy in Fig. 3a shows barely energy dissipating deformation mechanisms except two parallel streaks at room temperature, the toughened resin in Fig. 3b is traversed of river lines in almost 45° to the crack direction. This results from a material yield between the particles accompanied by a plastic zone that occurs around the crack tip. Comparing the dp values of neat epoxy with 7.7 μm–16.9 μm in the modified system, the shear yielding between the particles is an evident toughening mechanism.

At −50 °C, the fracture micrographs appearance changes drastically. The neat resin shows barely deformation or ruptures, thus results in a mirror-like surface. Moreover, the reduced interaction of the toughening agent with the matrix resin is visible by the disappearance of shear yielding in 45° to the crack propagation direction, which can also be quantified by a reduction of the plastic zone size as listed in Table 3. An enhanced fracture toughness compared to the neat resin can be referred

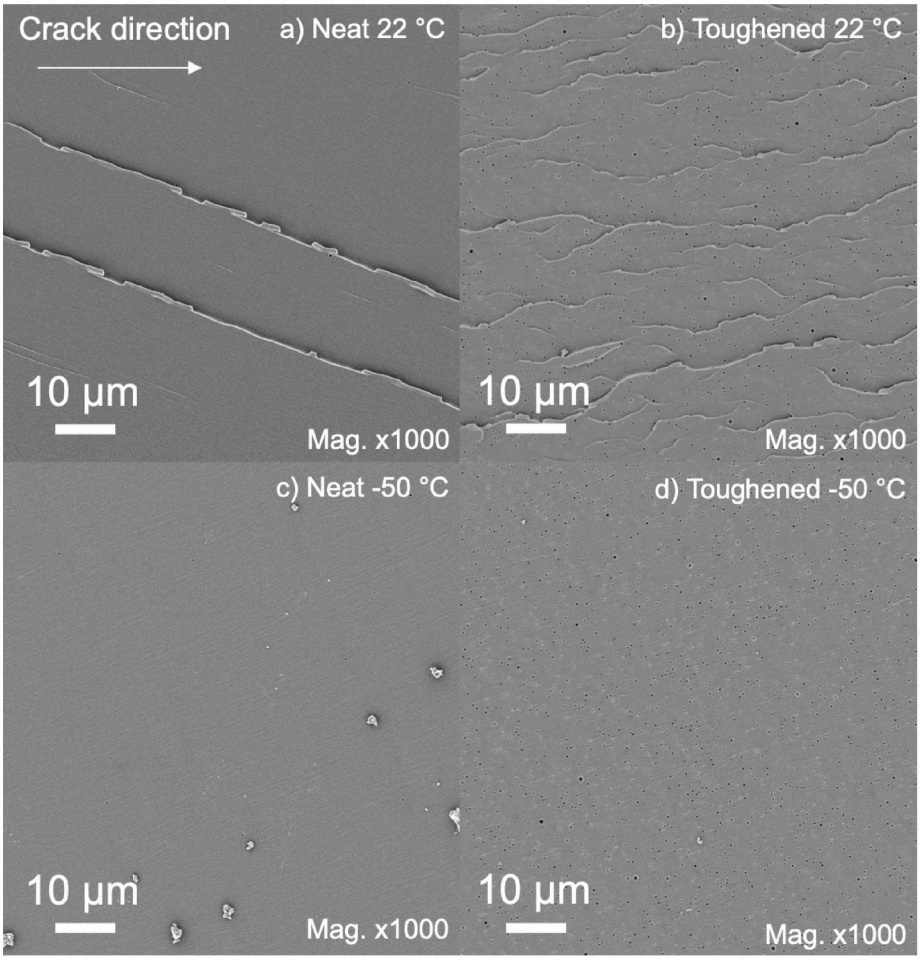


**Fig. 3.** KIC fracture micrographs of a) neat epoxy 22 °C b) toughened epoxy 22 °C c) neat epoxy −50 °C and d) toughened epoxy −50 °C taken with a backscattering electron (BSE) detector.

**Table 3**
Detailed data derived from KIC testing and related calculated values.

| | Testing Temperature | Neat 2100E + 2107H | Toughened 2100E + 2117H |
|---|---|---|---|
| Fracture toughness KIC [MPa m1/2] | +22 °C | 0.69 ± 0.04 | 1.05 ± 0.07 |
| Fracture energy GIC [J/m2] | +22 °C | 140.4 ± 16.7 | 316.0 ± 51.5 |
| Fracture toughness KIC [MPa m1/2] | - 50 °C | 0.83 ± 0.09 | 0.95 ± 0.05 |
| Fracture energy GIC ' [J/m2] | - 50 °C | 183.0 ± 37.9 | 239.44 ± 41.5 |
| Diameter plastic zone dp [µm] | +22 °C | 7.7 | 16.9 |
| Diameter plastic zone dp [µm] | −50 °C | 3.2 | 4.2 |

to partially occurring crack pinning effects. They appear behind the particles in a plain-strain-like crack front go-arounds and tailing which can be seen in Fig. 4b. These low temperature dissipation mechanisms increase the diameter of the plastic zone by 33% and $G_{IC}$ by 30%. This is a linear correlation since the crack fracture energy is related to the crack area.

Thus, an increased fracture energy of the neat sample at lower temperature is derived even though the diameter of the plastic zone is reduced. The dominant difference is highlighted in Fig. 4 with high magnification. Such phenomena can be concluded by the change in yield behavior, which is taken into account by compression tests for the calculation of $d_p$. An increased yield level as well as a change in Young's modulus at low temperatures described by DMA modify the behavior of the plastic zone drastically and result in vanishing shear yielding between the particles.

### 4.3. Fatigue crack propagation

According to [63], the fatigue crack propagation behavior of polymers can be divided in different segments, which are graphically highlighted in Fig. 5:

- Region I corresponds to the initiation of crack propagation starting with a threshold of $\boldsymbol{\Delta K_{threshold}}$.
- Region II concerns the zone in which a stable crack propagation is observed, and it is also called the Paris region.
- Region III regards the unstable crack growth which leads to failure of the probe and might be related to the materials inherent fracture toughness $K_{IC}$.

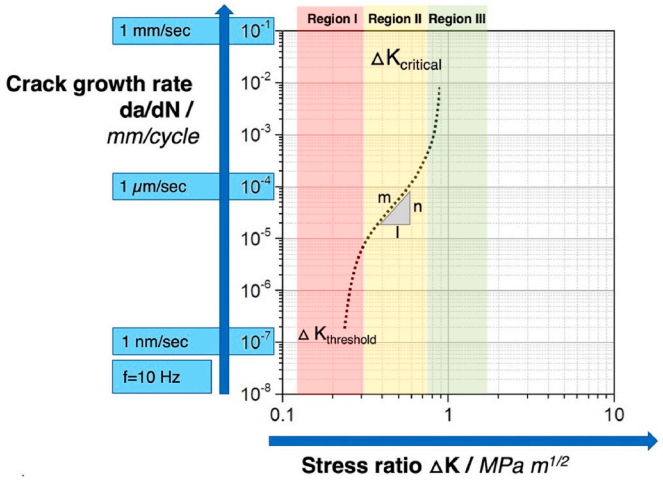


**Fig. 5.** *Schematic behavior of the three regions of fatigue crack propagation following* [64]. representing a naturally brittle EP resin's fatigue behavior.

The schematic presents the overall behavior in dependency of the testing frequency of 10 Hz. While EP resins and other thermosets do mostly not exceed a $K$ ratio of 1 MPa $m^{1/2}$, thermoplastic resin and other tough materials can vary up to 10 MPa $m^{1/2}$.

The characteristic fatigue propagation behavior of the neat and the toughened epoxy systems are compared. Thus, frequency of the mechanical testing of the samples, whether it's a short-term static or a long-term dynamic process, showed a huge influence on the fracture behavior. The fatigue crack growth rate per cycle $da/dN$ is plotted versus the ratio of the amplitude of the cyclic stress intensity factor $\Delta K$ in Fig. 6, which represents the $da/dN$ measurement of one representative out of the two carried out valid experiments. Table 4 shows the mean values of the maximum $K$ ratio, the low deviation of the curves expresses the precise measurement procedure.

Here the difference between the toughened and the non-toughened systems is clearly visible. While the light blue- and orange-colored curves fail earlier, the red and dark blue curves are representing the toughened system which show a visible shift to the right-hand side within higher $K$ ratios. Also, the light blue curve, neat EP at −50 °C, shows a higher crack propagation speed of almost one order of magnitude. This marks that the value of the BCP is increasing the fracture toughness during static as well as dynamic measurements. The neat epoxy resin at room temperature fails within a $\Delta K$ of 0.617 MPa $m^{1/2}$ while the toughened one at 0.754 MPa $m^{1/2}$ which expresses the successful proof of the BCP additives. At low temperature, the neat system

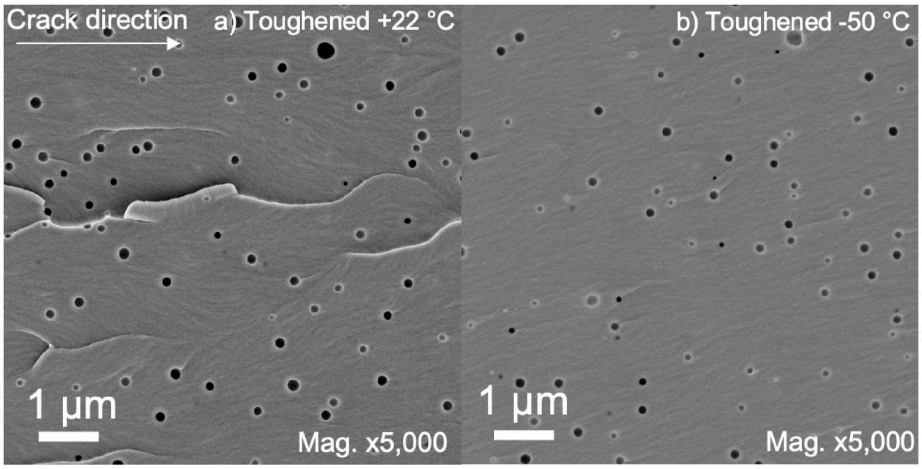


**Fig. 4.** *Fracture micrographs of a) Toughened epoxy at* 22 °C b*) Toughened epoxy at -50°C taken with a backscattering electron (SE) detector.*

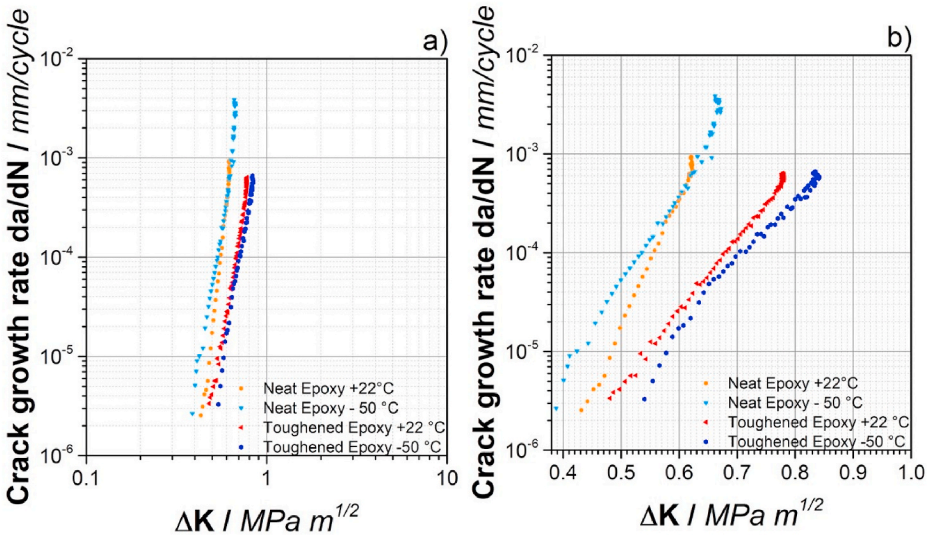


**Fig. 6.** *Fatigue crack propagation diagrams of toughened and non-toughened epoxy systems measured at 23 °C and -50 °C* - a) log-log scale and b) logarithmic versus magnified linear scale.

**Table 4**
Fatigue crack propagation testing relevant parameters and results.

| | | Non-Toughened 2100E + 2107H | Toughened 2100E + 2117H |
|---|---|---|---|
| ΔKmax | +22 °C | 0.617 ± 0.004 | 0.754 ± 0.03 |
| ΔKmax | −50 °C | 0.686 ± 0.02 | 0.839 ± 0.003 |
| da/dN at break [mm/cycle] | +22 °C | 9.282 × 10-4 | 6.2 × 10-4 |
| da/dN at break [mm/cycle] | −50 °C | 2.88 × 10-3 | 5.84 × 10-4 |
| Crack tip opening displacement $\delta$ [μm] | +22 °C | 1.46 | 2.40 |
| Crack tip opening displacement $\delta$ [μm] | −50 °C | 0.85 | 1.36 |
| Diameter plastic zone dynamic [μm] | +22 °C | 7.7 | 11.9 |
| Diameter plastic zone dynamic [μm] | −50 °C | 2.66 | 4.14 |
| Slope m Region II [a.u. x 10-6] | +22 °C | 3.086 | 1.415 |
| Slope m Region II [a.u. x 10-6] | −50 °C | 4.44 | 1.63 |

increases the ratio for the start of instable crack growth to 0.686 MPa $m^{1/2}$ while the toughened one now also increased the value to 0.839 $m^{1/2}$.

Also, the slope *m* of the curve changes, which leads to higher crack growth rates at higher *K* ratios. This contrary effect of increased crack growth rates is related to the effects of a higher modulus of the material and a general stiffening of the molecular bonds by network contraction. Furthermore, Fig. 6b magnifies the regions I and II which shows clearly the difference between the regions. Within the first 5 to 6 measurement points between a *K* ratio of 0.4–0.45, the slope of the curves is changed. This marks the threshold value to make the crack propagate stable in a log-log scale through the material. Moreover, the toughened system shows an interesting phenomenon at −50 °C which is described by the dark blue curve. In contrary to the neat epoxy, the crack growth rate before the instable region III is slightly lower. A crack growth rate at −50 °C of 5.84 mm/cycle compared to 22 °C with 6.2 mm/cycle indicates, that a superior material behavior is present. Not only that the crack propagates slower but also a higher number of cycles was necessary to reach instable crack growth in region III. The phenomena can be described by an overall changed interaction of the crack in the epoxy-BCP mixture. The lower deformation speed in *da/dN* (μm/sec) compared to $K_{IC}$ (mm/sec) leads to a way higher interaction of the toughened epoxy matrix. This results in higher energy dissipation and thus increased fracture toughness, respectively. The SEM micrographs in Fig. 7 support the theory, that the BCP toughener enhances the brittle epoxy resin performance drastically for both, 22 °C and −50 °C even though static measurements showed a drop in $K_{IC}$ stress scenario.

No shear yielding was found in static $K_{IC}$ testing at −50 °C, but the river lines return in *da/dN* testing. This phenomenon can be seen in Fig. 7a at 22 °C and 7b at −50 °C. This corresponds clearly to the increased *K* ratio of the toughened system at −50 °C. A higher energy dissipation leads to the assumption of a reverted interaction of the crack front with the toughener even under low temperature as long as the testing speed and *K* ratio does not exceed a certain level. Quasi-static $K_{IC}$ with 10 mm/min triggers a type of faster crack growth behavior than fatigue crack propagation investigations. Furthermore, Fig. 7c and d show clearly the effect of a low temperature embrittlement in the epoxy matrix itself, which is also described in literature [40,62] In between the particles, the neat epoxy does not tend to deform plastic any more at low temperature. Thus, it can be linked to a flat and smooth surface. Matrix shear yielding is no more visible at −50 °C, which is a minor energy dissipating mechanism. This explains clearly the matrix yielding in dependency of the specimen's temperature. The polymer segments show a lower movement and thus a higher stiffness. Since the beta-relaxation linked to the chain movement of the aromatic ring in the DGEBA structure is partially frozen at −50 °C, a direct link from matrix shear yielding to this molecular movement can be assumed. As seen from Table 4, also the calculated diameter of the plastic zone during crack propagation is changing. The neat system has a nearly constant $\Delta K_{max}$ value but $d_p$ changes drastically from 7.7 μm down to 2.66 μm in low temperature. By a modification of the neat resin, a drop from 16.9 μm to 11.9 μm is visible when comparing static and dynamic plastic zones. This is related to the testing procedure which results in different interaction speeds of the matrix with the tougheners. Nevertheless $d_p$ values calculated from static and dynamic experiments exhibit the same trend at both temperatures for both samples.

The overall behavior of the resins fatigue crack propagation behavior in regard to the effect of toughening and testing temperature are briefly summarized by comparing the parameter *m* as the slope of the curves. While *m* increases the neat systems crack propagation from 3.09 × $10^{-6}$ a.u. to 4.44 × $10^{-6}$ a.u. by 44% when testing in −50 °C, the toughened epoxy only increases by 15%. More interestingly, the slope m diminishes for both temperatures in presence of BCP toughener, which demonstrates clearly an enhancement of performance in fatigue behavior.

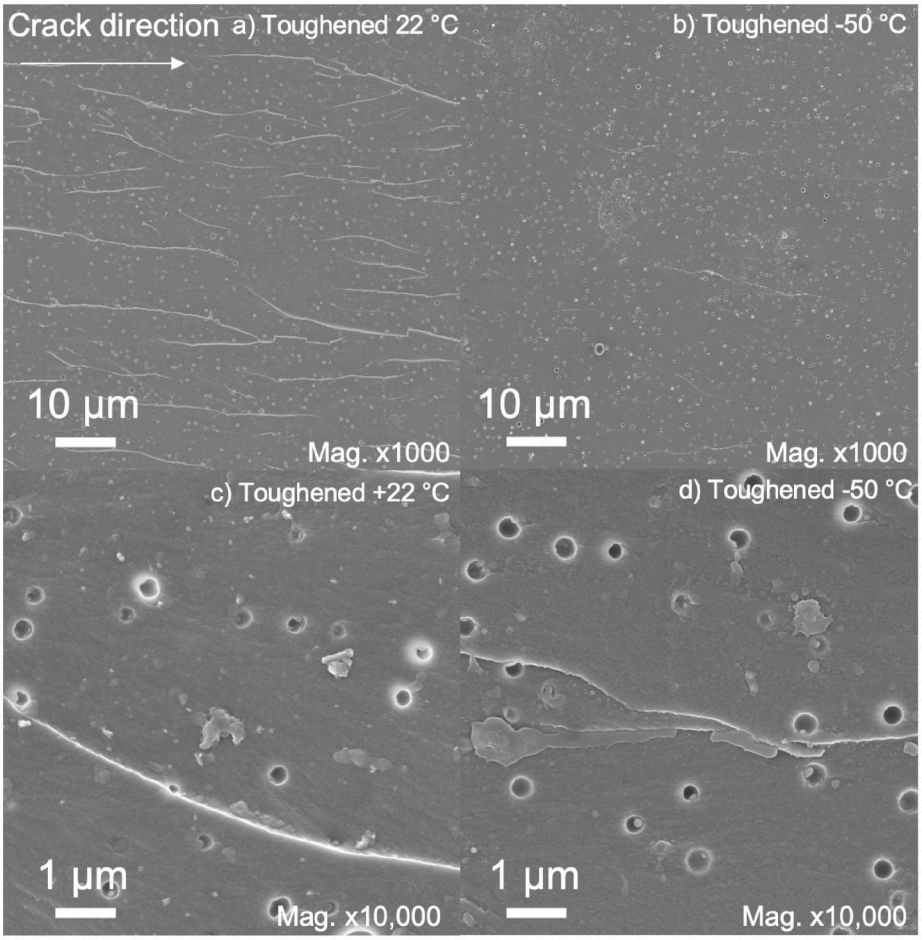


**Fig. 7.** *Fracture micrographs of* ***fatigue tested*** *a) and c) Toughened Epoxy* 22 °C b*) and d) Toughened epoxy at -50 °C taken with an Inlens detector.*

## 5. Conclusion

In this study a comparison of an application relevant liquid epoxy resin for liquid composite molding of composite parts in regard to the deformation and fracture behavior was carried out. The fatigue crack propagation behavior was investigated at +22 °C and −50 °C. The low temperature fracture toughness has a huge relevance e.g., for CFRP vessel's filling procedure of cryo-compressed hydrogen gas. The DMTA measurements revealed the high stiffening effect of epoxy at low temperatures as well as the remaining efficiency of the tougheners. Those positive effects were increasing network density as well as beta relaxation transition at around −50 °C of the aromatic epoxy groups. Moreover, $K_{IC}$ and *da/dN* were compared within the toughening mechanisms via SEM micrographs, both neat and toughened epoxy. A drastic increase of the functional properties like tensile and compression strength was demonstrated and the resulting material parameters like the evolution of the plastic zone in static and dynamic testing were calculated. Overall, the epoxy resins undergo a stiffening at −50 °C monitored by an increasing modulus and a decrease in the strain at break. The most important highlight from this study is derived from the calculation of the slopes of the fatigue curves. They reveal a dependency of the toughener's efficiency from the testing frequency: While $K_{IC}$ in static is generally improved in EP at −50 °C, the toughener seems to have no positive effect on the first view because $K_{IC}$ decreases back on the neat level. But, the *da/dN* testing and also the behavior of the plastic zone, which is dependend of the modulus brought the deepened understanding, that the crack growth rate is decreased drastically, when the material is toughened and undergoes low temperature stress. When it comes to the application of highly pressurized CFRP vessels, it is thus crucial to understand these failure phenomena in the composite, in order to prevent them from catastrophic failures.

### Author statementDeclaration of interests

☒ The authors declare have seen and approved the final version of the manuscript being submitted. They warrant that the article is the authors' original work, hasn't received prior publication and isn't under consideration for publication elsewhere.

### Credit author statement

Fabian Hübner, Alexander Brückner: Experimentation, Conceptualization, Methodology, Software, Data curation, Writing-Original draft preparation, Visualization, Investigation. Supervision, Writing-Reviewing, and Writing-Editing. Tobias Dickhut, Volker Altstädt, Agustín Rios de Anda, Holger Ruckdäschel: Conceptualization, Methodology, Software, Data curation, Writing-Original draft preparation, Visualization, Investigation. Supervision, Writing-Reviewing, and Writing-Editing.

### Declaration of competing interest

The authors declare that they have no known competing financial interests or personal relationships that could have appeared to influence the work reported in this paper.

## Acknowledgement

This work was supported by Research Foundation "Bayerische Forschungsstiftung (BFS). This publication was funded by the German Research Foundation (DFG) and the University of Bayreuth in the funding programme Open Access Publishing. Special thanks to Benjamin Benz (Blue Cube Germany Assets GmbH & Co.KG Olin Corporation) for providing sample material. Thanks to Johannes Meuchelböck, Andreas Mainz, Ute Kuhn and Annika Pfaffenberger for support of testing, thermal analysis and SEM micrographs.

## References

[1] L. Scelsi, M. Bonner, A. Hodzic, et al., Potential emissions savings of lightweight composite aircraft components evaluated through life cycle assessment, Express Polym. Lett. 5 (2011) 209–217, https://doi.org/10.3144/expresspolymlett.2011.20.
[2] A.T. Nettles, E.J. Biss, Low Temperature Mechanical Testing of Carbon-Fiber/epoxy-Resin Composite Materials - NASA Technical Paper, 1996.
[3] J. Hu, S. Sundararaman, K. Chandrashekhara, et al., Analysis of composite hydrogen storage cyclinders under transient thermal loads, Int. Conf. Hydrog. Saf. (2007).
[4] R.R. Barth, K.L. Simmons, C. San Marchi, Polymers for Hydrogen Infrastructure and Vehicle Fuel Systems, 1–51, Prod-Ng.Sandia.Gov, 2013. https://prod-ng.sandia.gov/techlib-noauth/access-control.cgi/2013/138904.pdf. (Accessed 14 February 2021). accessed.
[5] S. Sprenger, S. Sprenger, The effects of silica nanoparticles in toughened epoxy resins and fiber-reinforced composites. Eff. Silica Nanoparticles Toughened Epoxy Resins Fiber-Reinforced Compos, 2015, pp. 1–7, https://doi.org/10.3139/9781569906286.fm.
[6] F. Sawa, S. Nishijima, T. Okada, Molecular design of an epoxy for cryogenic temperatures, Cryogenics (Guildf). 35 (1995) 767–769, https://doi.org/10.1016/0011-2275(95)90910-8.
[7] G. Yang, S.Y. Fu, J.P. Yang, Preparation and mechanical properties of modified epoxy resins with flexible diamines, Polymer (Guildf) 48 (2007) 302–310, https://doi.org/10.1016/j.polymer.2006.11.031.
[8] R.A. Pearson, A.F. Yee, Toughening mechanisms in elastomer-modified epoxies - Part 3 the effect of cross-link density, J. Mater. Sci. 24 (1989) 2571–2580, https://doi.org/10.1007/BF01174528.
[9] A.J. Kinloch, F.J. Guild, Predictive Modeling of the Properties and Toughness of Rubber-Toughened Epoxies, 1996.
[10] F.J. Guild, A.J. Kinloch, A.C. Taylor, Particle cavitation in rubber toughened epoxies : the role of particle size, J. Mater. Sci. 45 (2010) 3882–3894, https://doi.org/10.1007/s10853-010-4447-y.
[11] A.J. Kinloch, R.D. Mohammed, A.C. Taylor, et al., The effect of silica nano particles and rubber particles on the toughness of multiphase thermosetting epoxy polymers, J. Mater. Sci. 40 (2005) 5083–5086, https://doi.org/10.1007/s10853-005-1716-2.
[12] B.B. Johnsen, A.J. Kinloch, R.D. Mohammed, et al., Toughening mechanisms of nanoparticle-modified epoxy polymers, Polymer (Guildf) 48 (2007) 530–541, https://doi.org/10.1016/j.polymer.2006.11.038.
[13] J.K. Huang, A, Kinloch, The role of plastic void growth in the fracture of rubber-toughened epoxy polymers, J. Mater. Sci. Lett. 11 (1992) 484–487, https://doi.org/10.1007/BF00731112.
[14] S. Sprenger, Improving mechanical properties of fiber-reinforced composites based on epoxy resins containing industrial surface-modified silica nanoparticles: review and outlook, J. Compos. Mater. 49 (2015) 53–63, https://doi.org/10.1177/0021998313514260.
[15] S. Sprenger, Epoxy resin composites with surface-modified silicon dioxide nanoparticles: a review, J. Appl. Polym. Sci. 130 (2013) 1421–1428, https://doi.org/10.1002/app.39208.
[16] T.H. Hsieh, A.J. Kinloch, K. Masania, et al., The mechanisms and mechanics of the toughening of epoxy polymers modified with silica nanoparticles, Polymer (Guildf) 52 (2010) 2518–2522, https://doi.org/10.1002/pen.23211.
[17] M. Iijima, M. Tsukada, H. Kamiya, Effect of particle size on surface modification of silica nanoparticles by using silane coupling agents and their dispersion stability in methylethylketone 307 (2007) 418–424, https://doi.org/10.1016/j.jcis.2006.11.044.
[18] J. Ebenoch, W. Ag, Tough and heat-resistant : new silicone particles for thermosets, Kunststoffe Plast Eur (2004) 1. –3, https://en.kunststoffe.de/a/specialistarticle/additives-tough-and-heat-resistant-new-s-261439. (Accessed 15 February 2021). accessed.
[19] H.R. Brown, J.A. Schneider, T.L. Murphy, Experimental studies of the deformation mechanisms of core-shell rubber-modified diglycidyl ether of bisphenol-A epoxy at cryogenic temperatures, J. Compos. Mater. 48 (2014) 1279–1296, https://doi.org/10.1177/0021998313485262.
[20] L. Becu, A. Maazouz, H. Sautereau, et al., Fracture Behavior of Epoxy Polymers Modified with Core-Shell Rubber Particles, 1996, pp. 2419–2431.
[21] S. Li, Q. Wu, H. Zhu, et al., Impact Resistance Enhancement by Adding Core-Shell Particle to Epoxy Resin Modified with Hyperbranched Polymer, Polymers (Basel), 2017, p. 9, https://doi.org/10.3390/polym9120684.
[22] S. Xing, J. Yang, C. Yin, et al., Preparation and Characterization of a Core-Shell Curing Agent for the Composite Repair Prepreg System, 2013, https://doi.org/10.1002/pc.
[23] F. Wolff-Fabris, V. Altstädt, Toughness modification of electron beam curable epoxy matrices for carbon fibre composites, Int. SAMPE Tech. Conf. (2010).
[24] J. Wang, D. Magee, J.A. Schneider, Dynamic mechanical properties and fracture surface morphologies of core-shell rubber (CSR) toughened epoxy at Liquid Nitrogen (LN2) temperatures, Int. SAMPE Symp. Exhib. 54 (2009) 12–13.
[25] M. Blanco, M. López, G. Kortaberria, et al., Nanostructured thermosets from self-assembled amphiphilic block copolymer/epoxy resin mixtures: effect of copolymer content on nanostructures, Polym. Int. 59 (2010) 523–528, https://doi.org/10.1002/pi.2731.
[26] Y. Meng, X. Zhang, Nanostructure Formation in Thermoset/Block Copolymer and Thermoset/Hyperbranched Polymer Blends, Elsevier Inc., 2013, ISBN 9781455731596, https://doi.org/10.1016/B978-1-4557-3159-6.00006-7.
[27] J Daniel Liu, H.J. Sue, Z.J. Thompson, et al., Effect of crosslink density on fracture behavior of model epoxies containing block copolymer nanoparticles, Polymer (Guildf) 50 (2009) 4683–4689, https://doi.org/10.1016/j.polymer.2009.05.006.
[28] M.A. Hillmyer, P.M. Lipic, D.A. Hajduk, et al., Self-assembly and polymerization of epoxy resin-amphiphilic block copolymer nanocomposites, J. Am. Chem. Soc. 119 (1997) 2749–2750, https://doi.org/10.1021/ja963622m.
[29] J. Liu, H.J. Sue, Z.J. Thompson, et al., Nanocavitation in self-assembled amphiphilic block copolymer-modified epoxy, Macromolecules 41 (2008) 7616–7624, https://doi.org/10.1021/ma801037q.
[30] Z.J. Thompson, M.A. Hillmyer, J. Liu, et al., Block copolymer toughened epoxy: role of cross-link density, Macromolecules 42 (2009) 2333–2335, https://doi.org/10.1021/ma900061b.
[31] P.M. Lipic, F.S. Bates, M.A. Hillmyer, Nanonstructured thermosets from self-assembled amphiphilic block copolymer/epoxy resin mixtures, J. Am. Chem. Soc. 120 (1998) 8963–8970, https://doi.org/10.1021/ja981544s.
[32] Y.X. He, Q. Li, T. Kuila, et al., Micro-crack behavior of carbon fiber reinforced thermoplastic modified epoxy composites for cryogenic applications, Compos. Part B Eng. 44 (2013) 533–539, https://doi.org/10.1016/j.compositesb.2012.03.014.
[33] M.G. Kim, J.S. Hong, S.G. Kang, et al., Enhancement of the crack growth resistance of a carbon/epoxy composite by adding multi-walled carbon nanotubes at a cryogenic temperature, Compos. Part A Appl. Sci. Manuf. 39 (2008) 647–654, https://doi.org/10.1016/j.compositesa.2007.07.017.
[34] R.A. Pearson, A.F. Yee, Toughening mechanisms in thermoplastic-modified epoxies: 1. Modification using poly(phenylene oxide), Polymer (Guildf). 34 (1993) 3658–3670, https://doi.org/10.1016/0032-3861(93)90051-B.
[35] J.F. Timmerman, B.S. Hayes, J.C. Seferis, Cryogenic microcracking of carbon fiber/epoxy composites: influences of fiber-matrix adhesion, J. Compos. Mater. 37 (2003) 1939–1950, https://doi.org/10.1177/0021998303036281.
[36] H. Nakane, S. Nishijima, H. Fujishiro, et al., Thermal Properties of Epoxy Resins at Cryogenic Temperatures, 2002, p. 211, https://doi.org/10.1063/1.1472545.
[37] A. Ahmed, R. Joven, R. Das, et al., Study of Thermal Expansion in Carbon Fiber Reinforced Polymer Composites, SAMPE Int. Symp. Proc. (n.d.).
[38] H. Cease, P.F. Derwent, H.T. Diehl, et al., Measurement of Mechanical Properties of Three Epoxy Adhesives at Cryogenic Temperatures for CCD Construction, 2006, pp. 1–19.
[39] J.W. Yi, Y.J. Lee, W. Lee, et al., Cryogenic Thermal Expansion and Mechanical Properties of Epoxy Rein Modified with Polydimethylsiloxane, 2012, pp. 24–28.
[40] F. Sawa, S. Nishijima, T. Okada, Molecular design of an epoxy for cryogenic temperatures, Cryogenics (Guildf). 35 (1995) 767–769, https://doi.org/10.1016/0011-2275(95)90910-8.
[41] R. Kulkarni, O. Ochoa, Transverse and longitudinal CTE measurements of carbon fibers and their impact on interfacial residual stresses in composites, J. Compos. Mater. 40 (2006) 733–754, https://doi.org/10.1177/0021998305055545.
[42] J.W. Bae, W. Kim, S.H. Cho, et al., Thermal fatigue-resistant EMCs (epoxy molding compounds) for microelectronic encapsulation, Korean J. Chem. Eng. 17 (2000) 41–46, https://doi.org/10.1007/BF02789251.
[43] P. Paris, F. Erdogan, A critical analysis of crack propagation laws, J. Fluids Eng. Trans. ASME. 85 (1963) 528–533, https://doi.org/10.1115/1.3656900.
[44] P.C. Paris, D. Lados, H. Tada, Reflections on identifying the real ΔKeffective in the threshold region and beyond, Eng. Fract. Mech. 75 (2008) 299–305, https://doi.org/10.1016/j.engfracmech.2006.12.029.
[45] J. Karger-Kocsis, K. Friedrich, Microstructure-related fracture toughness and fatigue crack growth behavior in toughened, anhydride-cured epoxy resins, Compos. Sci. Technol. 48 (1993) 263–272.
[46] M.H. Kothmann, R. Zeiler, A. Rios De Anda, et al., Fatigue crack propagation behaviour of epoxy resins modified with silica-nanoparticles, Polymer (Guildf) 60 (2015) 157–163, https://doi.org/10.1016/j.polymer.2015.01.036.
[47] G. Bakis, M.H. Kothmann, R. Zeiler, et al., Influence of size, aspect ratio and shear stiffness of nanoclays on the fatigue crack propagation behavior of their epoxy nanocomposites, Polymer (Guildf) 158 (2018) 372–380, https://doi.org/10.1016/j.polymer.2018.10.008.
[48] M.H. Kothmann, M. Ziadeh, G. Bakis, et al., Analyzing the influence of particle size and stiffness state of the nanofiller on the mechanical properties of epoxy/clay nanocomposites using a novel shear-stiff nano-mica, J. Mater. Sci. 50 (2015) 4845–4859, https://doi.org/10.1007/s10853-015-9028-7.
[49] A. Klingler, B. Wetzel, Fatigue crack propagation in triblock copolymer toughened epoxy nanocomposites, Polym. Eng. Sci. (2017), https://doi.org/10.1002/pen.24558.
[50] Blue Cube Germany Assets GmbH & Co.KG (Olin epoxy)., SDS Olin Epoxy Resin 2100E, (n.d.).

[51] Blue Cube Germany Assets GmbH & Co.KG (Olin epoxy)., SDS Olin Epoxy Resin 2117H, (n.d.).
[52] Blue Cube Germany Assets GmbH & Co.KG (Olin epoxy)., SDS Olin Epoxy Resin 2107H, (n.d.).
[53] H. Pham, US 2009/0123759 Amphiphillic Block Co-polymer-toughened Epoxy Resins and Adhesives Made Therefrom, 2009.
[54] G. Levita, S. De Petris, A. Marchetti, et al., Crosslink density and fracture toughness of epoxy resins, J. Mater. Sci. 26 (1991) 2348–2352, https://doi.org/10.1007/BF01130180.
[55] L. Monnerie, F. Lauprêtre, J.L. Halary, Investigation of solid-state transitions in linear and crosslinked amorphous polymers, Adv. Polym. Sci. 187 (2005) 35–213, https://doi.org/10.1007/b136955.
[56] J.N. Sultan, F.J. McGarry, Effect of rubber particle size on deformation mechanisms in glassy epoxy, Polym. Eng. Sci. 13 (1973) 29–34, https://doi.org/10.1002/pen.760130105.
[57] S. Kenig, Processing of Polymer Nanocomposites, Hanser Publishers, Munich, 2019, ISBN:ISBN: 978-1-56990-636-1; ISBN: 978-1-56990-635-4. doi:10.1533/9780857096258.1.95.
[58] G.W. Ehrenstein, G. Riedel, P. Trawiel, Thermal Analysis of Plastics - Theory and Practice, Hanser, Munich, Germany, 2004, ISBN 156990362X.
[59] F. Hübner, E. Szpoganicz, M. Demleitner, et al., Time domain 1 H NMR, thermomechanical, and rheology multiscale structural characterization of polydimethylsiloxane-toughened epoxy nanocomposites for liquid composite molding, ACS Appl. Polym. Mater. (2020), https://doi.org/10.1021/acsapm.0c00763.
[60] E.S. Zhavoronok, I.N. Senchikhin, O.A. Khlebnikova, et al., Relaxation transitions in mixed epoxy networks based on diane and aliphatic, Epoxy Resins 89 (2015) 715–723, https://doi.org/10.1134/S0036024415040305.
[61] G. Christoph, Bruchprozesse von Polymeren bei tiefen Temperaturen, 1996.
[62] Z. Zhang, D. Evans, Investigation of fracture properties of epoxy at low temperatures, Polym. Eng. Sci. 43 (2003) 1071–1080, https://doi.org/10.1002/pen.10091.
[63] J. Kallrath, V. Altstädt, J.P. Schlöder, et al., Analysis of fatigue crack growth behaviour in polymers and their composites based on ordinary differential equations parameter estimation, Polym. Test. 18 (1999) 11–35, https://doi.org/10.1016/S0142-9418(98)00004-X.